Insect Inspired Three Dimensional Centring

Luke Cole[1,2] luke@coletek.org
Nick Barnes[1] nick.barnes@nicta.com.au

[1]National ICT Australia (NICTA), Locked Bag 8001, Canberra, ACT 2601
[2]Australian National University ACT, 0200, Australia

Abstract

Navigating a robot through confined three-dimensional spaces, such as a helicopter flying within a building containing rooms and corridors, presents some obvious difficulties. This paper presents and experimentally verifies a biologically inspired technique that uses optical flow to perform three-dimensional centring in corridor-like environments. The experiments are performed on an omni-directional mobile robot, which has vertical motion for two fish-eye cameras mounted to provide almost 360° vision.

1 Introduction

The biological creatures of this world provide a great inspiration for the development of artificial creatures. Even the most simple creatures such as insects and other arthropods demonstrate an impressive ability to navigate their environment despite having relatively simple neural systems. Their ability shows insects have developed a robust and simplistic motion control system that are invaluable for robotic systems [Srinivasan *et al.*, 1999b].

Most insects perform this impressive navigation ability via closely coupling their actions and perception. Their perception has evolved eyes that provide sight over nearly the entire view-sphere. These specialized eyes provide an advantage to estimating self-motion [Fermuller and Aloimonos, 1998], which may be why flying creatures often have near-panoramic vision.

Most robot navigation involves environment reconstruction and map-building, such as simultaneous localization and mapping (SLAM), which is computationally expensive [Durrant-Whyte and Bailey, 2006]. For high-speed ground robots or a flying robot, reactive techniques are more suitable for closed loop control behaviours. Bio-inspired visual navigation provides efficient and robust navigation algorithms for robots, some of which have already been successfully implemented in robots [Argyros *et al.*, 2004; Iida, 2003; Hrabar *et al.*, 2005].

Three-dimensional corridor-centring applies to a robot that is able to move in three dimensions of translation, moving down a corridor that is constrained in two dimensions, and the robot is free to move in the third. Such a scenario occurs when a corridor is constrained in height as well as width, such as in an air duct.

This paper extends the classic example of bee-inspired corridor-centring that balances the optical flow between the left and right walls [Srinivasan *et al.*, 1999a]. We introduce balancing the optical flow between the top and bottom surfaces, which will provide three-dimensional corridor-centring. It also extends the standard divergent stereo case to work from a spherical camera model, and near full view sphere. Our goal is to support flying robots, to navigate corridor-like environments, such as investigating buildings, or even air ducts and underground sewers.

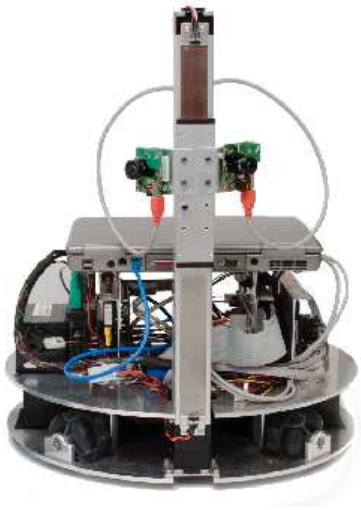

Figure 1: The InsectBot.

Ultimately three-dimensional corridor-centring should be trialled on a flying robot. However, testing such algorithms is difficult for the simple fact, if something goes wrong the flying robot could be damaged or destroyed. So algorithms for flying robots are generally developed using simulators such as: cable-array robots [Usher *et al.*, 2004]; gantry systems [Chahl and Srinivasan, 2000; Stürzl and Zeil, 2006]; and blimps [Iida and Lambrinos, 2000; van der Zwaan *et al.*, 2000]. However, gantry systems have limited workspaces, and exhibit very precise motion which is not a realistic simulation. Cable-array robots can not navigate through corridor-like environments. Blimps have a low acceleration and high inertia. Naturally a ground-based robot is more stable than a flying robot, but is somewhat more realistic than a gantry. It is for these reasons the InsectBot (Figure 1) was developed.

2 Research Platform: InsectBot

This paper presents an approach to three-dimensional centring using a novel platform (InsectBot) for flight simulation, which was briefly introduced in [Lim *et al.*, 2006]. This section provides more detail on the motion and perception of the InsectBot.

For flight simulation, the InsectBot provides four degrees of freedom (DOF) for the vision system, three in the horizontal plane and one in the vertical plane. Motion in the horizontal plane is performed using four omni-directional wheels, similar to [Huang *et al.*, 2004; Purwin and D'Andrea, 2005]. The motion in the vertical plane is performed using a custom lift-platform mechanism. However, for true flight simulation, the motion of the vision system should be extended to provide roll and pitch.

The vision system is comprised of stereo cameras fitted with hemispherical view ("fish-eye") lens, each providing 190° field of view. The stereo cameras and their fish-eye lens have been mounted so a small overlap exists between the cameras in the visual field. This overlap coupled with almost 360° field of view provides a vision system that is quite common among insects within the natural world [Lambrinos *et al.*, 2000].

This vision system and motion of the InsectBot allows for an ideal platform to research, among others, three-dimensional centring.

2.1 Kinematic Relationships

The general equation for the motion of an omni-directional wheel is [Ashmore and Barnes, 2002]:

$$V_w = V_b(cos(\theta)cos(\phi) + sin(\theta)sin(\phi)) + R\dot{\Psi} \quad (1)$$

where V_w is the velocity of the wheel, V_b is the velocity of the robot body, θ the reference wheel angle, ϕ is the reference body velocity angle, R is the distance of the wheel from the centre of mass, and $\dot{\Psi}$ is the rotational velocity.

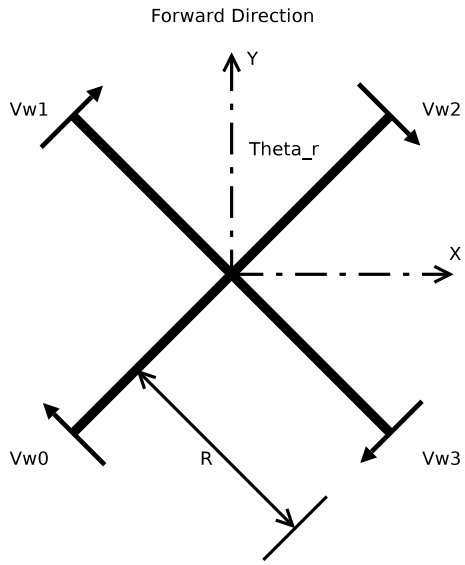

Figure 2: InsectBot Reference Diagram

Applying Equation 1 to four omni-drive wheels, each equally spaced, such as the InsectBot, one can derive:

$$\begin{bmatrix} V_{w1} \\ V_{w2} \\ V_{w3} \\ V_{w4} \end{bmatrix} = A \begin{bmatrix} \dot{x} \\ \dot{y} \\ \dot{\Psi} \end{bmatrix}, \begin{bmatrix} \dot{x} \\ \dot{y} \\ \dot{\Psi} \end{bmatrix} = A^{-1} \begin{bmatrix} V_{w1} \\ V_{w2} \\ V_{w3} \\ V_{w4} \end{bmatrix} \quad (2)$$

$$A = \begin{bmatrix} cos(\theta_r) & sin(\theta_r) & R \\ cos(\theta_r + 2\pi/N) & sin(\theta_r + 2\pi/N) & R \\ cos(\theta_r + 4\pi/N) & sin(\theta_r + 4\pi/N) & R \\ cos(\theta_r + 6\pi/N) & sin(\theta_r + 6\pi/N) & R \end{bmatrix} \quad (3)$$

where, V_{wM} is the velocity of wheel M, $\dot{x}$ and $\dot{y}$ are the robots velocities, N is the number of wheels and θ_r is the angle to reference vector. To take advantage of the Velocity Augmentation Factor (VAF) [Ashmore and Barnes, 2002] in the forward direction, the reference vector is defined as $\theta_r = 45°$ as depicted in Figure 2.

The vertical motion performed by the lift-platform is provided by a controller (Parker ViX250IE). This controller allows one to simply set the required motion profile (acceleration, velocity, deacceleration, position).

3 Approach

Previous approaches for two-dimensional centring [Coombs *et al.*, 1995; McCarthy and Barnes, 2004] define the horizontal heading direction to be simply:

$$\theta_h = K_h(\tau_l - \tau_r) \quad (4)$$

where, τ_l and τ_r are the average flow magnitudes in the left and right peripheral views, and K_h is the horizontal proportional gain.

So for three-dimensional centring we simply use the same equation, but for the vertical frame, giving:

$$\theta_v = K_v(\tau_b - \tau_t) \tag{5}$$

where, τ_b and τ_t are the average flow magnitudes in the bottom and top peripheral views. And K_v is the vertical proportional gain.

For Equations 4 and 5 to work the cameras need to be calibrated. So for a fish-eye camera calibration [Kannala and Brandt, 2006], the flow in the peripheral views is mapped to a sphere as shown in Figure 3.

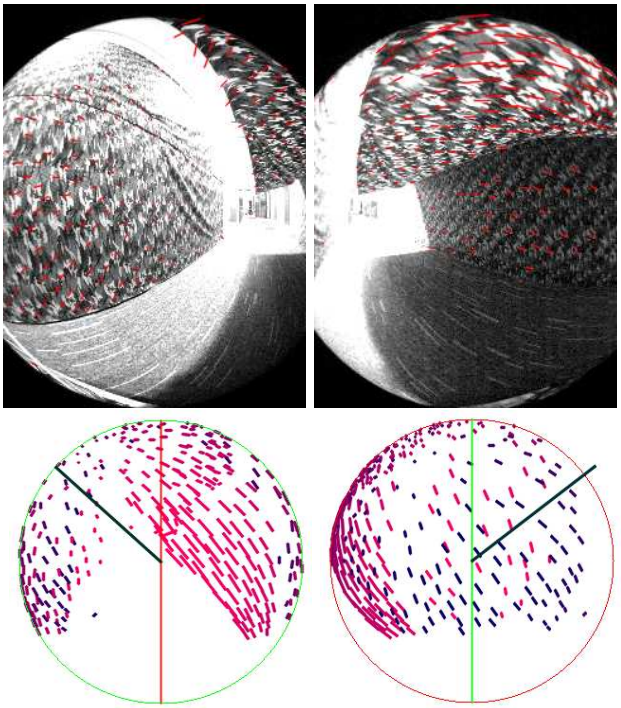

Figure 3: Mapped flow on sphere and heading direction vector. Top: Camera views. Bottom-Left: Top of sphere. Bottom-Right: Side of sphere. Red circle divides the left and right peripheral views, green circle divides the bottom and top peripheral views. The large vector shows the heading direction. The color of the vectors denote their depth, pink being near, blue being far.

For this approach, the flow for each peripheral view (τ) is taken to be a hemisphere. This is represented in Figure 3 by the red and green circles, where red divides the left and right peripheral views, and green divides the bottom and top peripheral views.

Another approach would be to use an area of each peripheral view, as opposed to the entire hemisphere. However, this would reduce peripheral information, and determining the location, size and shape of this area creates another unknown. A better approach would be, to reduce the horizontal and vertical flow interference, by using the following equations when determining the flow for each hemisphere:

$$\tau_l = \frac{\sum_{i=1}^{N_l}(||\overrightarrow{f_i}|||sin(\theta_i)|)}{N_l}, \tau_r = \frac{\sum_{i=1}^{N_r}(||\overrightarrow{f_i}|||sin(\theta_i)|)}{N_r} \tag{6}$$

$$\tau_t = \frac{\sum_{i=1}^{N_t}(||\overrightarrow{f_i}|||cos(\theta_i)|)}{N_t}, \tau_b = \frac{\sum_{i=1}^{N_b}(||\overrightarrow{f_i}|||cos(\theta_i)|)}{N_b} \tag{7}$$

where, $||\overrightarrow{f_i}||$ is the magnitude of the i^{th} flow vector, θ_i is the zenith angle to the start point of the i^{th} flow vector, and N_x is the number of flow vectors for hemisphere x.

So we will use Equations 6 and 7 for our experiments. And compare there response when these equations are not used.

It should be pointed out that the approach outlined in this section would fail for any rotations. This could be simply solved by subtracting the rotation of the robot from the flow vectors. The rotation of the robot could be determined by an accelerometer, gyroscope (for example [Hrabar *et al.*, 2005]), or ideally using optical flow itself (for example [Lim and Barnes, 2008]).

4 Experimental Procedure

We performed three-dimensional corridor centring experiments in an indoor corridor. However, due to the restricted vertical motion of the InsectBot, a low ceiling is required. The corridor in which the experiments are run has blank featureless walls and poor lighting, which does not produce good optical flow. We lined the walls and a false ceiling with textured material to ensure optical flow could be measured. Figure 4 shows the environment used for these results.

To analyse the performance of navigating through this environment, we performed eight trials. Four trials using the environment shown in Figure 4, with two different starting positions at the entrance. The other four trials use the same environment without the ceiling, again with two different starting positions at the entrance. For each set of trials we present two graphs, which will show the desired horizontal and vertical angles to navigate. We also show a series of images for one run through each environment.

5 Results

We conducted two sets of experiments with full three dimensional control of centring using Equations 6 and

Figure 4: The environment for experimental trials. Left: Entrance. Right: Exit.

Start Time (s)	End Time (s)	Environment
0	22	Wide straight textured corridor with declining ceiling.
22	30	Narrowing corridor.
35	40	Narrow straight corridor.

Table 1: Time-line for graphs presented.

7 for control. In the first experiments (trials 0-3), the robot moved down the environment shown in Figure 4. This has two textured walls, where the right hand wall narrows late in the corridor, and a textured ceiling that declines smoothly. The approximate temporal sequence of events as the robot moves down this corridor in the experiments is shown in Table 1. Figures 5 and 6 show the graphs of the horizontal and vertical behaviour. The plot is over time taken for the whole experiment - with evenly paced motion, and the angle shows the change in angle horizontally in Figure 5, and vertically in Figure 6. In the second set of experiments (trials 4-7) the ceiling was removed. Figures 7 and 8 show the horizontal and vertical motion for this scenario respectively. The final set of experiments (trials 8-11), are a repeat the first set of experiments, however without using Equations 6 and 7. Figures 9 and 10 show the horizontal and vertical motion for this scenario respectively.

Analysing Figures 5 and 7, we see approximately the same behaviour. Initially the robot steers left (given a right starting position at the entrance) or right (given a left starting position at the entrance). Once the robot reaches the center of the wide corridor, its horizontal motion remains approximately zero. At the narrowing corridor, the robot steers left to enter the narrow corridor. While entering the narrow corridor, we see some overshoot causing the robot to steer right to centre itself.

Analysing Figures 6 and 8, we see a distinct difference as expected by the change in environment: Figure 8 shows the vertical motion to be steady, while Figure 6 shows a decreasing vertical motion, due to the declining ceiling. Figure 6 also shows an increasing vertical motion as the ceiling passes. After the ceiling has passed, we see both Figures 6 and 8 exhibit the same behaviour. That is, an increasing vertical motion, since there is no ceiling.

The benefits of Equations 6 and 7 can be seen by analysing Figures 9 and 10. Here we see some interesting behaviour during motion through the narrowing corridor. The vertical oscillating behaviour seen in Figure 10, is due to the horizontal motion from the narrowing wall, inducing vertical flow (and hence the vertical motion). Similarly, the horizontal overshooting seen in Figure 9, is caused by the vertical flow from the declining ceiling.

Experimental trial 0 is shown in video [Luke Cole, 2008a]. Experimental trial 7 is shown in Figure 11 and video [Luke Cole, 2008b]. Experimental trial 8 is shown in Figure 12 and video [Luke Cole, 2008c]. These figures and videos demonstrate the behaviour discussed above. In particular, Figure 12 and video [Luke Cole, 2008a] show the vertical centring of the stereo cameras, while Figure 11 and video [Luke Cole, 2008b] show the horizontal centring of the robot.

Overall we see a smooth controlled motion in response to the changes in the shape of the corridor in three dimensions. We see the advantages of Equations 6 and 7 in terms of eliminating interference in the vertical control by changes in the horizontal corridor, and vice versa. Significant oscillations in the motion are removed by the introduction of these equations.

6 Conclusion

The algorithm presented and experimented in this paper produced a accurate and smooth response to the changes in the shape of the textured environment. So this approach could be used for flying vehicles, to navigate three-dimensional corridor-like environments. However, before the system can be used on a real flying vehicle the algorithm needs to handle roll, pitch and rotations.

7 Future Work

- Extend algorithm to handle roll and pitch.
- Extend algorithm to handle rotations.
- Test the algorithm on a flying vehicle.

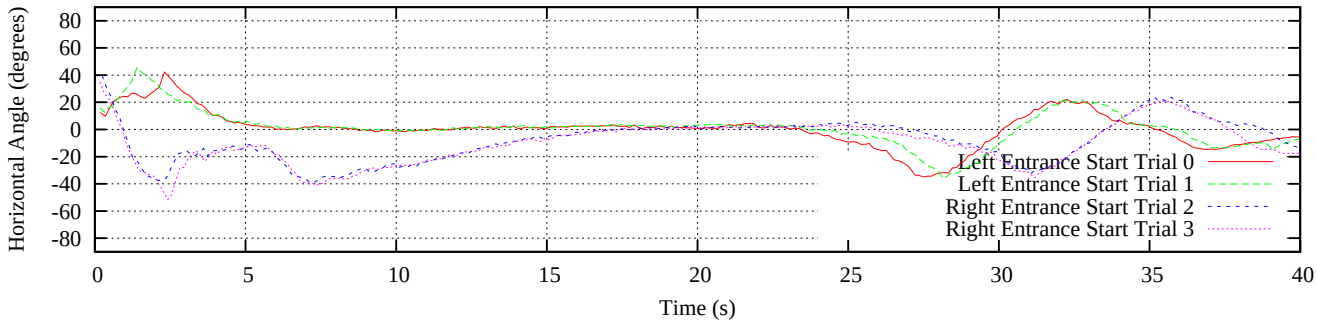

Figure 5: θ_h for trials with declining ceiling. See Table 1 for a description of the timeline.

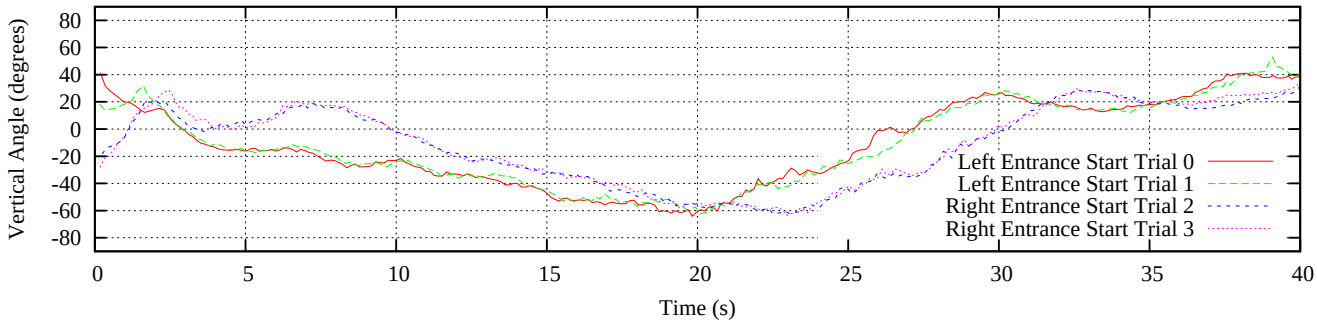

Figure 6: θ_v for trials with declining ceiling. See Table 1 for a description of the timeline.

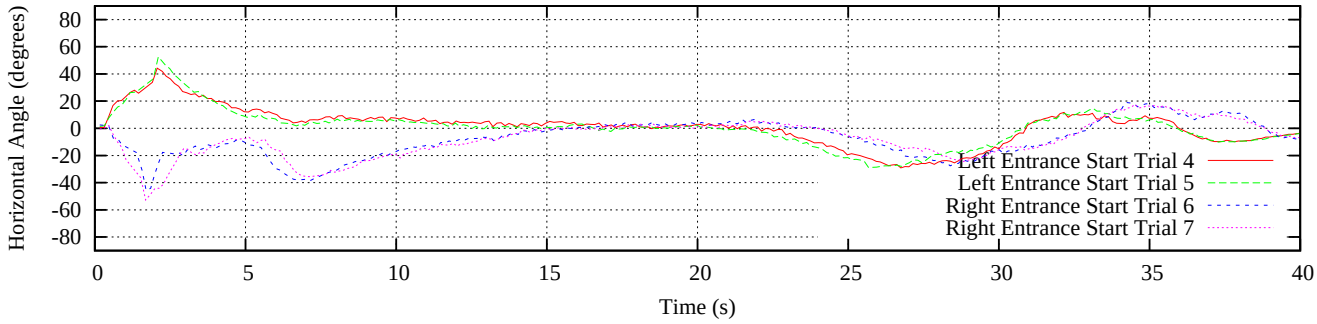

Figure 7: θ_h for trials without ceiling. See Table 1 for a description of the timeline.

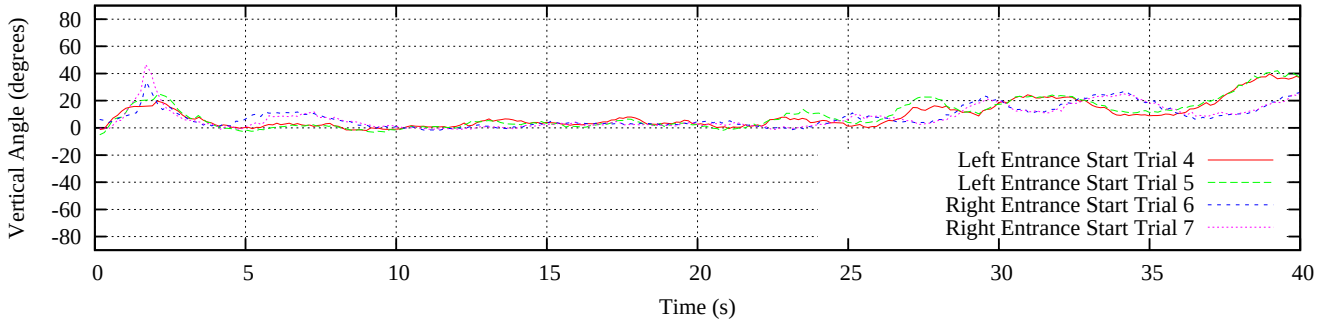

Figure 8: θ_v for trials without ceiling. See Table 1 for a description of the timeline.

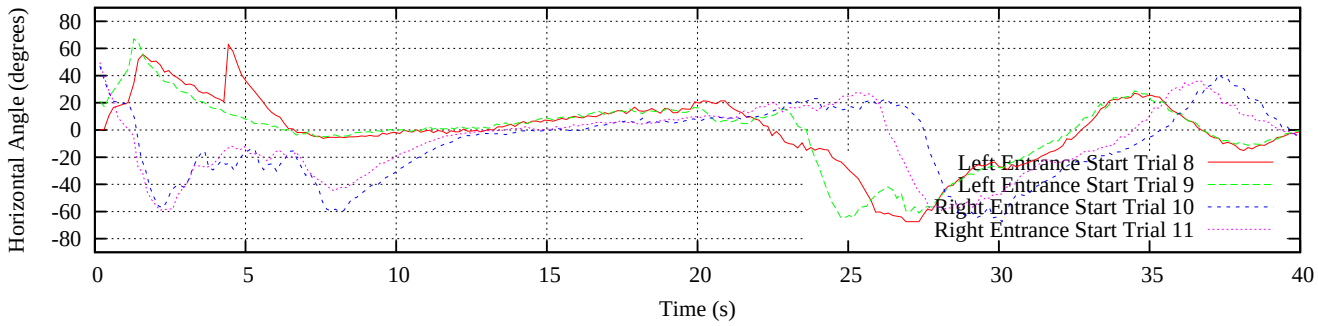

Figure 9: θ_h for trials with declining ceiling, without using Equations 6 and 7. See Table 1 for a description of the timeline.

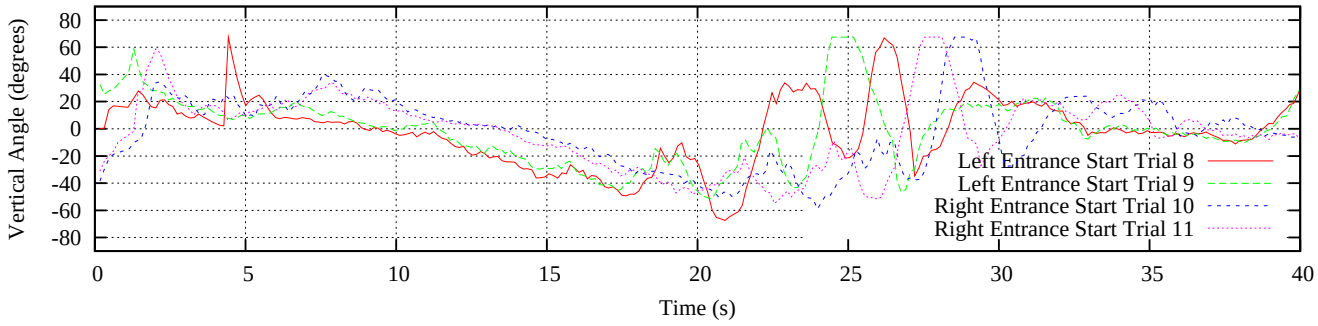

Figure 10: θ_v for trials with declining ceiling, without using Equations 6 and 7. See Table 1 for a description of the timeline.

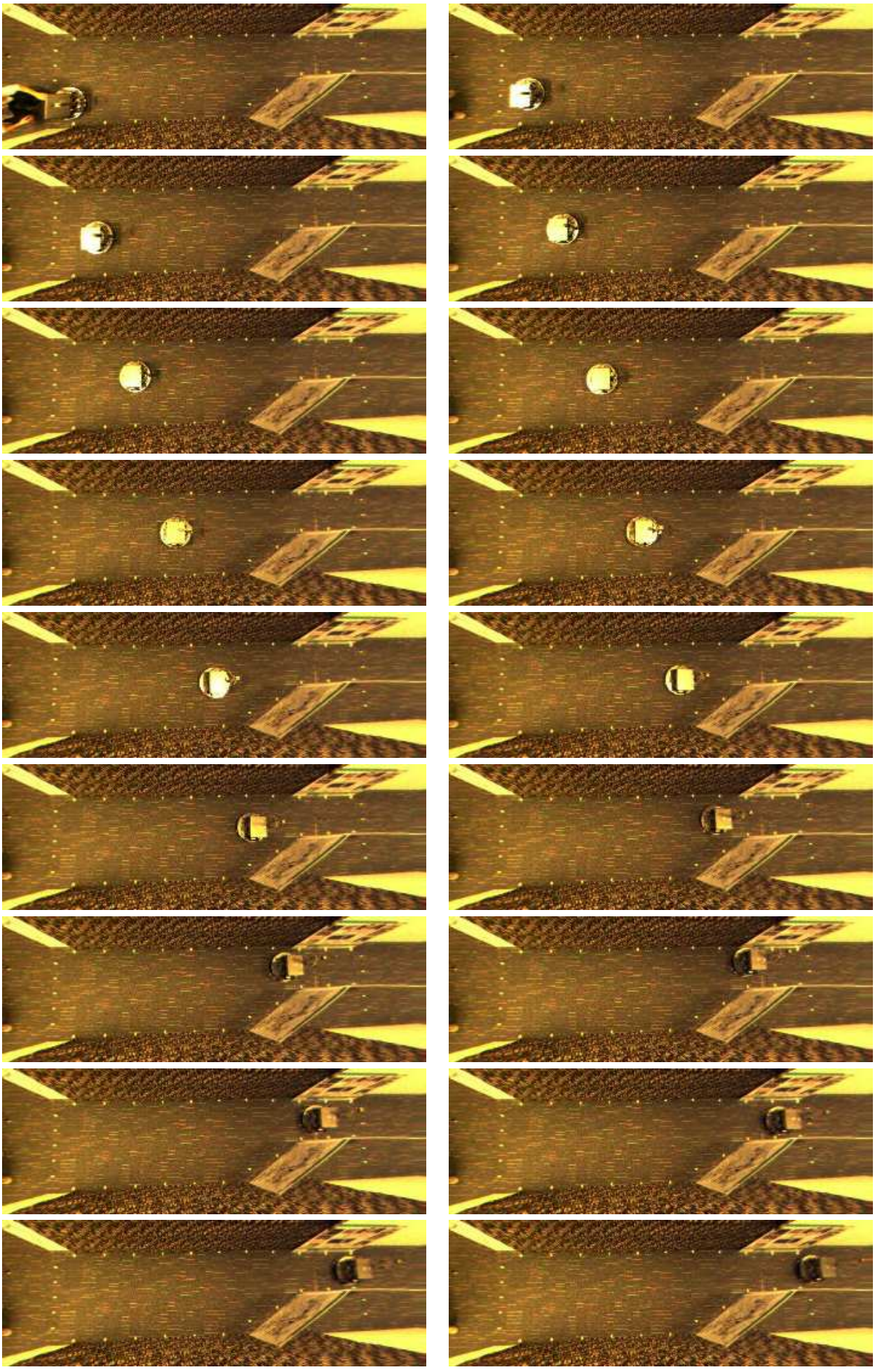

Figure 11: Image frames from experimental trial 7. Frames are ordered left to right, top to bottom.

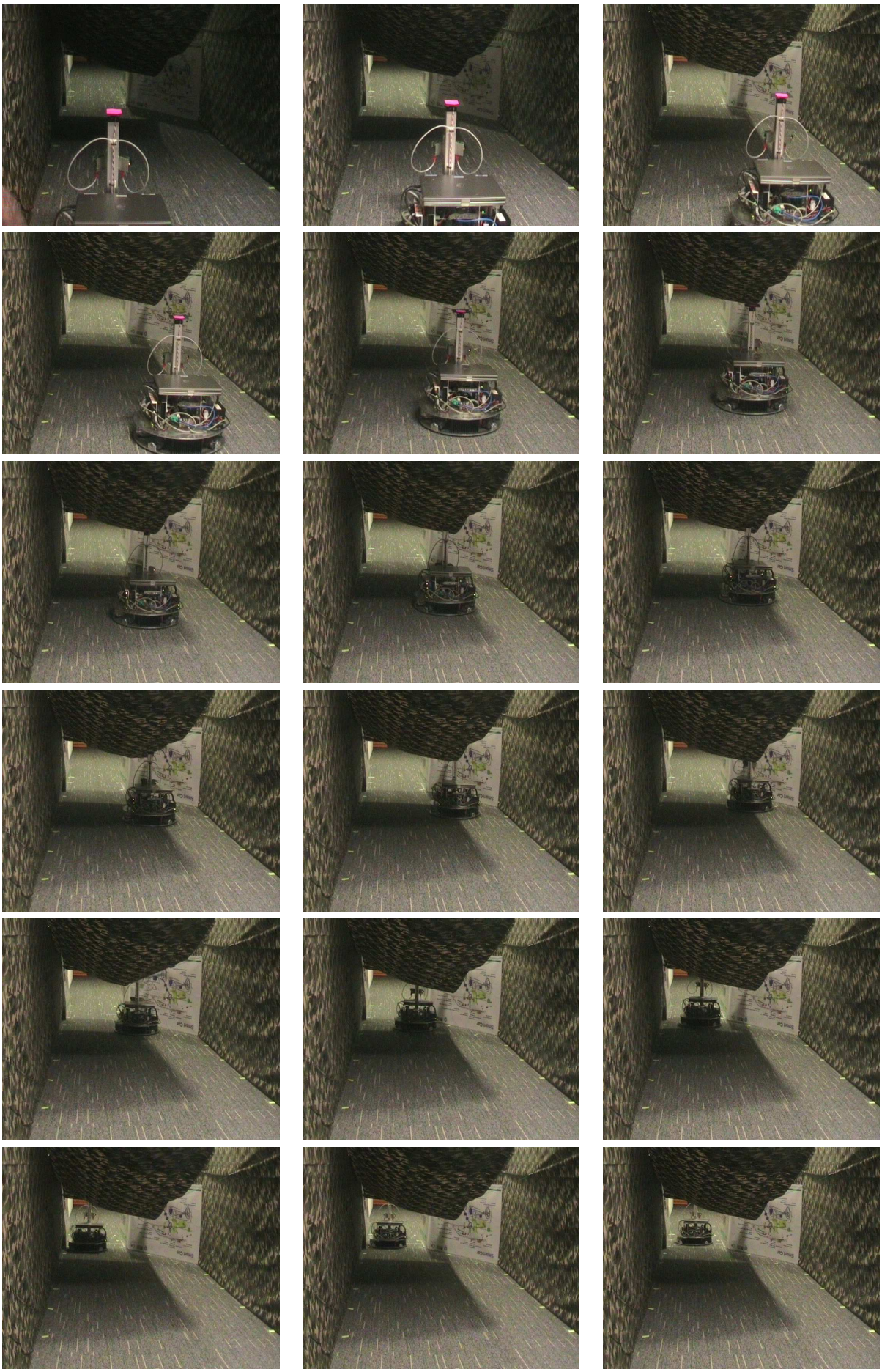

Figure 12: Image frames from experimental trial 8. Frames are ordered left to right, top to bottom.

8 Acknowledgements

Part of this work was supported by funding from NICTA. NICTA is funded by the Australian Government as represented by the Department of Broadband, Communications and the Digital Economy and the Australian Research Council through the ICT Centre of Excellence program.

References

[Argyros *et al.*, 2004] A.A. Argyros, D.P. Tsakiris, and C. Groyer. Bio-mimetic centering behavior: Mobile robots with panoramic sensors. *IEEE Robotics and Automation Magazine, Special Issue on Panoramic Robotics*, 11(2):21–30, 2004.

[Ashmore and Barnes, 2002] Mark Ashmore and Nick Barnes. Omni-drive robot motion on curved paths: The fastest path between two points is not a straight-line. In *Proc. of the National Conference on Artificial Intelligence*, pages 225–236, December 2002.

[Chahl and Srinivasan, 2000] J. S. Chahl and M. V. Srinivasan. A complete panoramic vision system, incorporating imaging, ranging, and three dimensional navigation. In *OMNIVIS '00: Proceedings of the IEEE Workshop on Omnidirectional Vision*, page 104, Washington, DC, USA, 2000. IEEE Computer Society.

[Coombs *et al.*, 1995] D. Coombs, M. Herman, Tsai Hong, and M. Nashman. Real-time obstacle avoidance using central flow divergence and peripheral flow. *ICCV*, 00:276, 1995.

[Durrant-Whyte and Bailey, 2006] H. Durrant-Whyte and T. Bailey. Simultaneous localization and mapping. *IEEE Robotics and Automation Magazine*, pages 99–108, 2006.

[Fermuller and Aloimonos, 1998] C. Fermuller and Y. Aloimonos. Ambiguity in structure from motion: Sphere versus plane. *International Journal of Computer Vision*, 28:137–154, 1998.

[Hrabar *et al.*, 2005] Stefan Hrabar, Gaurav Sukhatme, Peter Corke, Kane Usher, and Jonathan Roberts. Combined optic-flow and stereo-based navigation of urban canyons for a uav. In *Proc. Int. Conf on Intelligent Robots and Systems (IROS)*, Alberta, August 2005.

[Huang *et al.*, 2004] L. Huang, Y.S. Lim, David Li, and Christopher E. L. Teoh. Design and analysis of a four-wheel omnidirectional mobile robot. In *The second International Conference on Autonomous Robots and Agents*, December 2004.

[Iida and Lambrinos, 2000] Fumiya Iida and Dimitrios Lambrinos. Navigation in an autonomous flying robot by using a biologically inspired visual odometer. In *Sensor Fusion and Decentralized Control in Robotic System III, Photonics East, Proceeding of SPIE*, volume 4196, pages 86–97, 2000.

[Iida, 2003] F. Iida. Biologically inspired visual odometer for navigation of a flying robot. *Robotics and Autonomous Systems*, 44(3-4):201–208, 2003.

[Kannala and Brandt, 2006] Juho Kannala and Sami S. Brandt. A generic camera model and calibration method for conventional, wide-angle, and fish-eye lenses. *IEEE Transactions on Pattern Analysis and Machine Intelligence*, 28(8):1335–1340, 2006.

[Lambrinos *et al.*, 2000] D. Lambrinos, R. Moller, T. Labhart, R. Pfeifer, and R. W ehner. A mobile robot employing insect strategies for navigation. *IEEE Transactions on Robotics and Autonomous Systems*, 30(1):39–64, 2000.

[Lim and Barnes, 2008] John Lim and Nick Barnes. Directions of egomotion from antipodal points. *IEEE International Conference on Computer Vision and Pattern Recognition (CVPR)*, June 2008.

[Lim *et al.*, 2006] John Lim, Chris McCarthy, David Shaw, Nick Barnes, and Luke Cole. Insect inspired robots. *Proceedings of Australian Conference on Robotics and Automation*, 2006.

[Luke Cole, 2008a] Luke Cole. 3d centring trial 0, 2008. http://insectbot.rsise.anu.edu.au/pub/media/research/acra2008/insectbot-trial0-video1.mpg.

[Luke Cole, 2008b] Luke Cole. 3d centring trial 7, 2008. http://insectbot.rsise.anu.edu.au/pub/media/research/acra2008/insectbot-trial7-video2.mpg.

[Luke Cole, 2008c] Luke Cole. 3d centring trial 8, 2008. http://insectbot.rsise.anu.edu.au/pub/media/research/acra2008/insectbot-trial8-video3.mpg.

[McCarthy and Barnes, 2004] C. McCarthy and N. Barnes. Performance of optical flow techniques for indoor navigation with a mobile robot. In *International Conference on Robotics and Automation (ICRA Q04)*, pages 5093–5098, 2004.

[Purwin and D'Andrea, 2005] Oliver Purwin and Raffaello D'Andrea. Trajectory generation for four wheeled omnidirectional vehicles. In *Proceedings of the American Control Conference*, volume 7, pages 4979–4984, June 2005.

[Srinivasan *et al.*, 1999a] M.V. Srinivasan, J.S. Chahl, K. Weber, S. Venkatesh, M .G. Nagle, and S.W. Zhang. Robot navigation inspired by principles of insect vision. *Robotic Autonomous Systems*, 26(2-3):203–216, 1999.

[Srinivasan *et al.*, 1999b] M.V. Srinivasan, J.S. Chahl, K. Weber, S. Venkatesh, M.G. Nagle, and S.W. Zhang. Robot navigaton inspired by principles of insect vision. *Journal of Robotics and Autonomous Systems*, 1999.

[Stürzl and Zeil, 2006] W. Stürzl and J. Zeil. Depth, contrast and view-based homing in outdoor scenes. *Biological Cybernetics*, pages 519–531, 2006.

[Usher *et al.*, 2004] Kane Usher, Graeme Winstanley, and Peter Corke. A cable-array robot for air vehicle simulation. In N. Barnes and D. Austin, editors, *Proceedings of the Australian Conference on Robotics and Automation*, Canberra, Australia, December 2004. CDROM. ISBN: 0958758360.

[van der Zwaan *et al.*, 2000] Sjoerd van der Zwaan, Alexandre Bernardino, and Jose Santos-Victor. Vision based station keeping and docking for an aerial blimp. In *IEEE/RSJ International Conference on Intelligent Robots and Systems (IROS)*, 2000.